Applied Materials Today 1 (2015) 80–87

Contents lists available at ScienceDirect

Applied Materials Today

journal homepage: www.elsevier.com/locate/apmt

Synergistic antibacterial activity of PEGylated silver–graphene quantum dots nanocomposites

Khaled Habiba[a,b,*], Dina P. Bracho-Rincon[b,c], Jose A. Gonzalez-Feliciano[b,c], Juan C. Villalobos-Santos[b,d], Vladimir I. Makarov[a], Darinel Ortiz[d], Javier A. Avalos[b,e], Carlos I. Gonzalez[b,c,f,g], Brad R. Weiner[b,g,h], Gerardo Morell[a,b,g]

[a] Department of Physics, University of Puerto Rico – Rio Piedras Campus, San Juan, PR 00936-8377, USA
[b] Molecular Sciences Research Center, University of Puerto Rico, 1390 Ponce de Leon Ave., STE. 2, San Juan, PR 00926-2614, USA
[c] Department of Biology, University of Puerto Rico – Rio Piedras Campus, San Juan, PR 00931-3360, USA
[d] Department of Biology, University of Puerto Rico – Bayamon Campus, Bayamon, PR 00959, USA
[e] Department of Physics, University of Puerto Rico – Bayamon Campus, Bayamon, PR 00959, USA
[f] Department of Biochemistry, University of Puerto Rico – Medical Sciences, San Juan, PR 00936-5067, USA
[g] Institute for Functional Nanomaterials, University of Puerto Rico, San Juan, PR 00931-3334, USA
[h] Department of Chemistry, University of Puerto Rico – Rio Piedras Campus, San Juan, PR 00931-3346, USA

ARTICLE INFO

Article history:
Received 4 August 2015
Received in revised form 5 October 2015
Accepted 5 October 2015

Keywords:
Graphene quantum dots
Antibacterial nanoparticles
Nanocomposites
Toxicity
Silver nanocomposites

ABSTRACT

The emergence of antibiotic-resistant bacteria is a major threat to world-wide public health. Functionalized nanoparticles could offer novel strategies in this post-antibiotic era. In this study, we developed nanocomposites of silver nanoparticles decorated with graphene quantum dots (Ag-GQDs) using pulsed laser synthesis. The nanocomposites were PEGylated, which increases their biocompatibility and solubility in aqueous solutions. The HR-TEM micrographs of bare GQDs show that their size is in the range of 1.6–4 nm, and the lattice spacing is 0.214 nm, which corresponds to the (1 0 0) lattice fringes of graphene. The antibacterial activity of Ag-GQDs was evaluated and compared to that of bare GQDs and commercial silver nanoparticles (Ag-NPs) against both Gram-negative and Gram-positive bacteria, using *Pseudomonas aeruginosa* and *Staphylococcus aureus* as model bacteria, respectively. Concentration values of 25 and 50 μg/mL are required for Ag-GQDs to inhibit the growth of *S. aureus* and *P. aeruginosa* bacteria, respectively. The fractional inhibitory concentration (FIC) index is below 0.5 indicating that there is a synergistic effect between Ag-NPs and GQDs. Kirby–Bauer tests showed that Ag-GQDs inhibit *P. aeruginosa* and *S. aureus*, in contrast to bare GQDs and Ag-NPs alone. Cell viability of normal mammalian cells treated with Ag-GQDs showed that cell viability is maintained at 100% for cells incubated with Ag-GQDs. The decoration of Ag-NPs with GQDs minimizes their cytotoxicity in mammalian cells and increases their biocompatibility. Ag-GQDs have potential applications in the fabrication of antibacterial coatings, self-sterile textiles, and personal care products.

1. Introduction

Microbial infections are considered a major health problem with a growing concern toward those that do not respond to treatment due to antibiotic-resistant bacteria. According to the U.S. Centers for Disease Control and Prevention, approximately two million people are infected annually with bacteria resistant to antibiotics, of which *ca.* 23,000 people die as a direct result of these infections [1]. The prevention and treatment of these infections has drawn considerable attention and presents a critical challenge to develop drugs, antibiotics and/or antibacterial substances able to inhibit bacterial growth.

Infections due to *Pseudomonas aeruginosa* (*P. Aeruginosa*) and *Staphylococcus aureus* (*S. aureus*) have been documented in surgical sites, where they have been attributed to dermal injuries and burn wounds [2]. Gram-negative bacteria are characterized by a lipid-rich outer membrane as well as a plasma membrane and a thin peptidoglycan layer, while Gram-positive bacteria are enshrouded in thicker, more resilient cell walls [3]. This difference in cell wall is important for antibiotic development, since bacterial resistance might be due in part to cell wall composition [4].

* Corresponding author at: Department of Physics, University of Puerto Rico, Rio Piedras Campus, San Juan, PR 00936-8377, USA.
E-mail addresses: khabiba@gmail.com, khaled.habiba@upr.edu (K. Habiba).

http://dx.doi.org/10.1016/j.apmt.2015.10.001

Several traditional antibacterial agents, such as: tetracycline, streptomycin, and sulfonamides, have been developed to inhibit bacterial infections. However, these antibiotics have failed to inhibit many types of bacteria and multidrug-resistant strains have appeared due to the pathogen's evolution in counteracting the biocidal action of the agent molecules [5]. Consequently, it is necessary to develop antibacterial agents that can overcome the limitations of common traditional antibacterial agents and preferably work against both types of bacteria. Emerging materials such as: silver nanoparticles (Ag-NPs) [6–13], copper oxide nanoparticles [13,14], carbon nanomaterials [15–20], and metal oxide nanoparticles [21], have been reported as antimicrobial agents. Specifically, silver is widely recognized for its capacity to kill bacteria and have been considered for use in wound infections and in the clothing industry [13,22,23], and products containing silver nanoparticles such as Acticoat wound dressing and I-Flow catheter were approved by the FDA [24]. Chemical and physical factors associated with Ag-NPs such as: their size [6,7], shape and surface charge [25] enhance their antibacterial properties and affect significantly the effective doses to inhibit bacterial growth. The mechanism of Ag-NPs as an antibacterial agent is not totally clear, but some possible mechanisms has been reported include: denaturation of the 30s ribosomal subunits [12], inhibition of respiratory enzymes [12,26], binding and dimerization of RNA and DNA [11], and disruption of the outer membrane [9]. Nevertheless, commercially available silver-based dressings have shown cytotoxic effects on various experimental models [10,27]. The synthesis of silver nanocomposites may be a potential solution to enhance the antibacterial activities of Ag-NPs and to overcome the adverse toxic effects of silver by optimizing the concentration of Ag. One approach to synthesize silver nanocomposites is to use carbon-based nanomaterials such as: graphene [28], carbon nanotubes (CNTs) [29–33], and graphene oxide with low concentrations of silver [33–37]. Seo et al. reported the synthesis and use of silver-CNTs complexes as antibacterial material [31]. Dong et al. showed that there is a synergistic effect between Ag-CNTs nanocomposites and oxidizing agents such (*i.e.*, H_2O_2 and NaOCl) when they are used in combination to treat Gram-positive and Gram-negative bacteria [29]. However, CNTs might be toxic due to their contamination with metallic catalysts used in their synthesis [36], and many reports have shown their potential hazards against mammalian cells [38–42]. Poland et al. reported that CNTs could be a potential carcinogenic material, and may lead to mesothelioma [41]. Liu et al. found that CNTs increase the intracellular reactive oxygen species (ROS), and can react with cellular macromolecules including DNA, proteins, and lipids and disturb the homeostasis of the intracellular milieu [40]. Graphene oxide–silver nanocomposite has also demonstrated antibacterial activity against *Escherichia coli* and *S. aureus*, however, they showed toxic effect against mammalian cells [43]. Therefore, there still much efforts needed and challenges to optimize these nanocomposites prior clinical use.

Graphene quantum dots (GQDs) are among the carbon nanostructures that may be good candidates for biomedical applications due to their solubility in aqueous solutions and high biocompatibility. GQDs are nanostructures of graphene in the size range of 2–20 nm with a set of excellent and unique chemical and physical properties [19,20,44–53]. In general, GQDs have no apparent toxicity [44,48,50,52], and they have demonstrated high potential for utilization in cellular imaging [46–48,52], as antibacterial material [19,20], and drug delivery [53]. Chong et al. studied their toxicity and biodistribution *in vitro* and *in vivo*, and analysis of WST-1 assay, cell apoptosis, LDH production and ROS level clearly demonstrated good biocompatibility of GQD and GQD-PEG at cellular level [44]. Nurunnabi et al. showed that carboxylated GQDs do not cause apparent toxicities in rats at different dosage (5 and 10 mg/kg) for 22 days as evidenced by blood biochemistry and hematological analysis [48].

Another proposed strategy to reduce the cytotoxicity of nanoparticles is the PEGylation of their surface [54]. The PEGylation is a process that involves the passivation of the surface of nanoparticles by polyethylene glycol (PEG), a coiled polymer PEG is a polymer of repeating ethylene ether units soluble in water and aqueous solutions, which reduce the tendency of nanoparticles to agglomeration and their interaction reticuloendothelial system *i.e.*, macrophages and monocyte, and increase their circulation time in blood. Interestingly, Marslin et al. reported that membrane permeabilizing nature of PEG would facilitate the entry of nanoparticles carrying antibiotics, enhance the binding of the delivered drug to the bacterial DNA and block drug efflux pumps [55]. We report hereby the synthesis of PEGylated Ag-GQDs nanoparticles and a study of their cell toxicity and antibacterial properties. By decorating Ag-NPs with GQDs, it is anticipated that the resulting Ag-GQDs can be tailored to be an efficient and a safe antibacterial material.

2. Materials and methods

2.1. Synthesis of the bare GQDs

For the synthesis of bare GQDs, we used our bottom-up synthesis approach as described previously [46]. To functionalize the synthesized bare GQDs with polyethylene glycol (PEG), we modified the irradiated mixture as follows. A 0.25 wt.% mixture of nickel oxide powder (Alfa Aesar) and 1.25 wt.% of PEG bis (3-aminopropyl) terminated (Sigma–Aldrich) in 98.5 wt.% benzene (Sigma–Aldrich) was irradiated for 45 min with a 1064 nm pulsed Nd:YAG laser (Continuum Surelite II, KDP doubling crystal, 10 Hz, 10 ns pulse width). The synthesized GQDs were separated from benzene and the precipitated nickel oxide by centrifugation at 10,000 rpm, after being dissolved in nano-pure water. Finally, the GQDs solution was purified using dialysis bags with a cut-off molecular weight (MWCO) of 6–8 kDa (Spectrum Labs, USA).

2.2. Synthesis of the bare GQDs and Ag-GQDs

For synthesis of Ag-GQDs, we have employed our approach to synthesize GQDs by pulsed laser [56] with minor modifications. Briefly, a mixture of 0.25 wt.% of silver powder (silver nanopowder No. 576832, Sigma–Aldrich) and 1.25 wt.% of PEG bis(3-aminopropyl) terminated (Sigma–Aldrich) in 98.5 wt.% benzene (Sigma–Aldrich) was prepared and irradiated by pulsed laser. After irradiation a mixture of GQDs and Ag-GQDs is formed in benzene. The synthesized nanoparticles were separated from benzene by vacuum evaporation and dissolved in nano-pure water, upon centrifugation at 10,000 rpm to precipitate the Ag-GQDs. After centrifugation, the Ag-GQDs were separated from free GQDs and excess of PEG by using dialysis bags with a cut-off molecular weight (MWCO) of 12–14 kDa (Spectrum Labs, USA).

2.3. Instrumentation and measurements

High transmission electron microscopy (HR-TEM) images were recorded using an electronic microscope (JEOL JEM-2200FS, Japan), operated at 200 kV in scanning transmission electron microscope (STEM) mode. XPS experiments were performed with Physical Electronics Instruments (PHI-Quantum 2000, USA), using Al K_α source. XRD patterns were performed with a powder diffractometer (Rigaku Smart-lab, Japan), equipped with a Cu K_α radiation source, at an accelerating potential of 40 kV and a tube current of 44 mA. The XRD samples were prepared by placing a certain powder amount of: bare GQDs, silver, or Ag-GQDs on silicon substrates. The hydrodynamic size of the Ag-GQDs nanocomposites and bare

silver nanoparticles were determined by dynamic light scattering (DLS) using a (Malvern Zetasizer Nanoseries, UK). The samples were dispersed in phosphate buffered saline solution (PBS) at 7.4.

2.4. Antibacterial tests

The antibacterial properties of the nanomaterials were tested against *P. aeruginosa* bacteria (ATCC 27853) and *S. aureus* bacteria (ATCC 25923). The inoculum for antibacterial assays was prepared from actively growing organisms (logarithmic phase). The inoculum of *S. aureus* and *P. aeruginosa* were prepared from an overnight culture grown aerobically in Mueller–Hinton (MH) broth at 37 °C. The bacterial concentration was determined by measuring optical density at 600 nm (OD_{600}).

2.4.1. The microdilution method

The bacterial minimum inhibitory concentration (MIC) for Ag-GQDs and GQDs were determined based on the broth microdilution methods, as described in the Clinical laboratory standards guidelines with minor modifications [57]. MIC is defined as the lowest concentration of an antimicrobial that will inhibit the visible growth of a microorganism after overnight incubation [58]. Briefly, bacterial suspensions were prepared from overnight cultures and adjusted to 10^6 CFU/mL. Then, a 100 μL of fresh MH broth, 40 μL of bacterial suspension and 60 μL of different concentrations of Ag-GQDs (1, 2, 25, 50, 100, 150, 200, 400 μg/mL), bare Ag-NPs (1, 2, 25, 50, 100, 150, 200 μg/mL) and bare GQDs (50, 100, 500, 700 and 900 μg/mL) were added in 96-well plate. A positive growth control of basal medium without nanoparticles was included to evaluate the viability of the tested organisms. The microplates were incubated aerobically at 37 °C for 24 h under linear shaking. Finally, the MIC value was determined by observing the wells corresponding to the lowest concentration inhibiting the bacterial growth. To determine if there is a synergistic effect between the GQDs and Ag-NPs in the Ag-GQDs nanocomposites, we applied the fractional inhibitory concentration (FIC) test [59]. The combined antibacterial effect of nanoparticles A and B (where A is Ag-NPs, B is GQDs, and AB is Ag-GQDs) was calculated as follows: the FIC index = [MIC(AB)/MIC(A)] + [MIC(AB)/MIC(B)]. FIC index values above 2.0 indicate antagonistic effects, values between 0.5 and 2.0 indicate additive effects, and values lower than 0.5 indicate synergistic effects. Note that we calculated the upper bound of the FIC index because we have available the lower bounds of MIC(A) and MIC(B).

2.4.2. Time-dependent growth inhibition assay

The bacterial population growth rate of bacteria treated with Ag-GQDs, GQDs or Ag-NPs was analyzed using the microplate reader (Biotek Synergy H4 Hybrid, Winooski, VT, USA). Bacterial suspensions were prepared from overnight cultures and adjusted to 10^6 CFU/mL. A 100 μL of fresh MH broth, 40 μL of bacterial suspension and 60 μL of different concentrations of Ag-GQDs (10, 25, 50, 100 and 150 μg/mL), bare Ag-NPs (10, 25, 50, 100 and 150 μg/mL), or GQDs (50, 100, 500, 700 and 900 μg/mL) were added in the 96-well microplate. For positive growth controls, 60 μL of nanoparticles were replaced with the solvent used to dissolve nanoparticles phosphate buffer saline (PBS). The absorbance was measured at OD_{600} at intervals of 20 min for a total period of 22 h.

2.4.3. The Kirby–Bauer disk diffusion method

The antimicrobial susceptibility of Ag-GQDs nanoparticles was evaluated using the Kirby–Bauer disk diffusion method [57]. In brief, a bacterial inoculum with a turbidity equivalent to 0.5 MacFarland was inoculated evenly onto the surface of MH agar in Petri dishes by swabbing. Sterile filter paper disks were impregnated with GQDs (100 μg/disk), bare Ag-NPs (50 and 100 μg/disk), or Ag-GQDs (50 and 100 μg/disk) and then deposited on the agar surface. For positive inhibition controls, disks of commercial antibiotics of streptomycin (10 μg/disk) and ampicillin (30 μg/disk) were used against *S. aureus*, and for *P. aeruginosa* disks of streptomycin (10 μg/disk) and tetracycline (30 μg/disk) were used. For negative inhibition controls, disks were impregnated with sterile PBS. The zones of inhibition were measured after 24 h of incubation at 37 °C.

2.4.4. SEM imaging of P. aeruginosa treated with Ag-GQDs

Prior to SEM analysis, samples of bacteria treated with Ag-GQDs, and untreated bacteria were prepared. Briefly, a drop of *P. aeruginosa* (10^6 CFU/mL) incubated with Ag-GQDs (25 μg/mL) or untreated bacteria was deposited on the surface of a sterile cover glass and incubated for 24 h at 37 °C inside an empty Petri dish. Both samples were dried and covered with a gold film of 10 nm using an Auto Sputter Coater Pelo SC-7. Finally, the samples were imaged with a FE-SEM (JEOL JSM-7500F, Japan) at an acceleration voltage of 15 kV.

2.5. Cell culture

HeLa cells were cultured in Eagle's minimum essential medium (ATCC) supplemented with 10% fetal bovine serum (ATCC), 100 U/mL penicillin, 100 μg/mL streptomycin and 250 ng/mL amphotericin B (Cellgro) at 37 °C with 5% CO_2.

Vero cells (African green monkey kidney epithelial cells; obtained from the Center for Disease Control and Prevention-Dengue Branch) were maintained in M199 medium (Mediatech) containing 5% heat-inactivated FBS, 1% sodium bicarbonate, 1% HEPES buffer, 1% glutamine and 1% penicillin–streptomycin at 5% CO_2 and 37 °C.

Jurkat cells were cultured in RPMI (ATCC) supplemented with 10% fetal bovine serum (ATCC), 100 U/mL penicillin, 100 μg/mL streptomycin and 250 ng/mL amphotericin B (Cellgro) at 37 °C with 5% CO_2.

2.6. MTS cell viability assay

The cell viability effects of GQDs, Ag-NPs and Ag-GQDs nanoparticles were assessed on Vero cells by using the (3-(4,5-dimethylthiazol-2-yl)-5-(3-carboxymethoxyphenyl)-2-(4-sulfophenyl)-2H-tetrazolium)-based (MTS) CellTiter 96® AQueous Solution Cell proliferation Assay (Promega, USA). 2×10^4 cells were seeded in 96-well plates (Falcon) and grown overnight. After 24 h, the cell culture medium was removed and 100 μL of complete cell medium containing Ag-GQDs, Ag-NPs or GQDs at the concentrations (25, 50, 100, 150 μg/mL) were added. Fresh culture medium was used as a negative control. After 24 h of cell incubation, the medium was discarded and 100 μL of fresh cell medium with 20 μL of MTS reagent was added. Then, the cells were incubated for 30 min at 37 °C and centrifuged at 1400 rpm for 5 min. Subsequently, the cell medium containing the MTS reagent was transferred to a new microplate and the absorbance at 490 nm was measured with a UV–vis microplate spectrometer (Biotek Synergy H4 Hybrid, Winooski, VT, USA).

Cell viability assays were assessed in Jurkat and HeLa cells for Ag-GQDs nanoparticles at the concentrations (25, 50, 100 and 150 μg/mL) using the (MTS) CellTiter 96® AQueous Solution Cell proliferation Assay. For HeLa, 2×10^4 cells were seeded in 96-well plates and for Jurkat 2×10^5 cells were seeded in 96-well plates (Falcon) and grown overnight. Fresh culture medium was used as a negative control. After 24 h of cells incubation, the medium was discarded and 100 μL of fresh cell medium with 20 μL of MTS reagent was added. Then, the cells were incubated for 30 min at 37 °C and centrifuged at 1400 rpm for 5 min. Subsequently, the cell medium containing the MTS reagent was transferred to

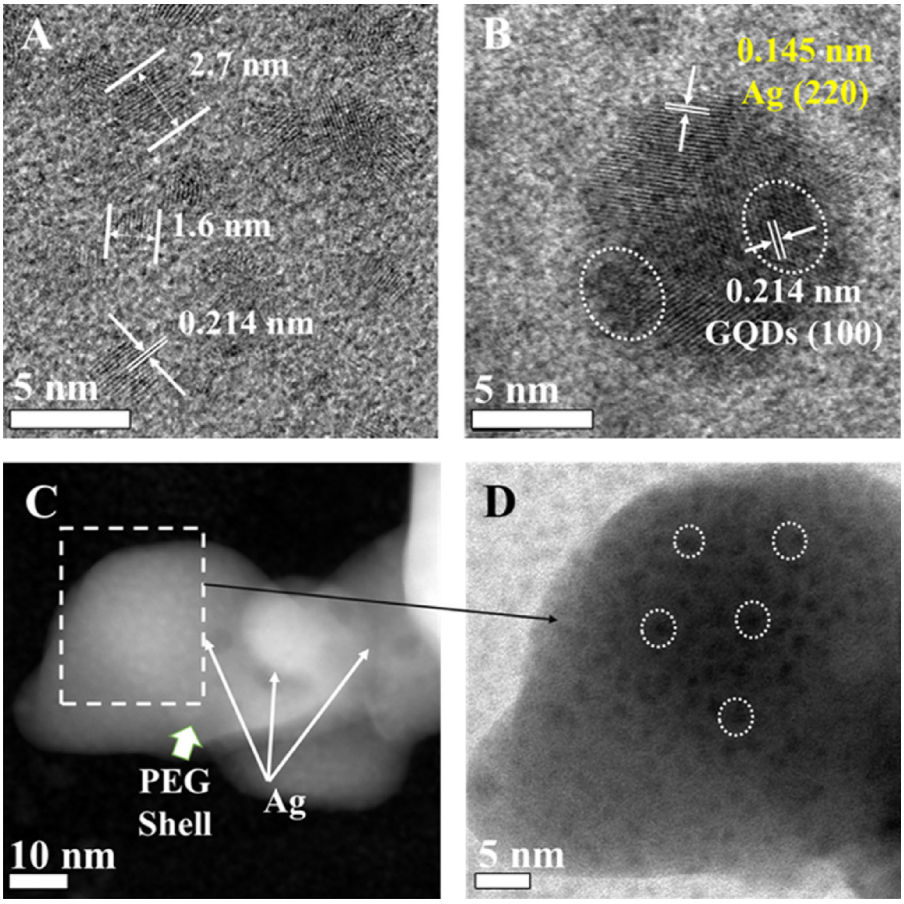

Fig. 1. HR-TEM image in scanning mode of (A) bare GQDs. (B) Magnified Ag-GQDs. (C) Magnified image of the Ag-GQDs cluster in dark-field, which shows the Ag-GQDs nanoparticles packed together inside the PEG shell. (D) Magnified image of the selected area in C, which shows GQDs inside the PEG shell. (For interpretation of the references to color in the text, the reader is referred to the web version of this article.)

a new microplate and the absorbance at 490 nm was measured with a UV–vis microplate spectrometer (Biotek Synergy H4 Hybrid, Winooski, VT, USA). For data analysis, the results were expressed as % of cell viability. The equation used was the following:

$$\%\ \text{of cell viability} = \frac{\text{Abs}_{490}\ \text{of treated cells}}{\text{Abs}_{490}\ \text{of untreated cells}} \times 100$$

2.7. Statistical analysis

The experiments were performed in triplicates. The results were expressed as the mean of the standard deviation of values obtained from at least three independent experiments, differences in mean between control and bacteria treated with each nanoparticle were analyzed by Student's t-test using GraphPad Prism 5 software and ($p < 0.05$) was considered statistically significant.

3. Results and discussion

3.1. Characterization of Ag-GQDs

The synthesized Ag-GQDs nanocomposites were fully characterized using microscopic and spectroscopic techniques, before studying its antibacterial activity. HR-TEM microscopy was employed to give information related to the size, morphology and crystalline structure of Ag-GQDs. The HR-TEM micrographs of bare GQDs (Fig. 1A) depict their size range of 1.6–4 nm, and lattice spacing of 0.214 nm that corresponds to the (1 0 0) lattice fringes of graphene [46,49]. Fig. 1B displays a single Ag-GQDs nanoparticle. The nanocomposites shows a diameter of 10 nm with an interplanar spacing of 0.145 nm (pointed out in yellow) that matches with the (2 2 0) plane of silver [32]. Some nanostructures were observed on the surface of the Ag-NPs with a lateral diameter of 1.6–2 nm and the same 0.214 nm (pointed out in white) interplanar spacing of graphene (1 0 0) shown in Fig. 1A. In order to obtain more information about the nanocomposites, we employed the dark field to get the high contrast of the clusters (Fig. 1C). The image in the inset (Fig. 1C) shows clusters of nanoparticles in the range of 50–70 nm and other nanoparticles less than 20 nm. It can be clearly observed that the nanoparticles of silver and GQDs are packed together forming the core, which is coated by the PEG shell. Fig. 1D confirms the presence of bare GQDs inside the PEG shell, when the selected region in the dotted rectangle (Fig. 1C) was magnified.

XRD spectroscopy was analyzed to reveal the crystalline structure of Ag-GQDs and validate the HR-TEM characterization results. XRD patterns were obtained for the bare GQDs, silver powder used in the synthesis, and the Ag-GQDs (Fig. 2). In the XRD pattern of silver, the peaks at 38.1°, 44.3°, 64.5° and 77.5° are assigned to the crystallographic planes (1 1 1), (2 0 0), (2 2 0) and (3 1 1) of the face-centered cubic (fcc) Ag nanoparticles, respectively, according to the JCPDS card No. 04-0783. For the bare GQDs, the peak at 26.6° is commonly observed and corresponds to the d-spacing of the basal plane (0 0 2) of graphite [51]. The peaks shown at 18.97°, 23.3° and 35.7° are attributed to PEG, which is conjugated on the surface of bare GQDs, and match with the PEG peaks reported by El Moussaoui et al. [60]. As expected, the combination of the observed peaks in silver, PEG and GQDs in the XRD pattern arise in the pattern of

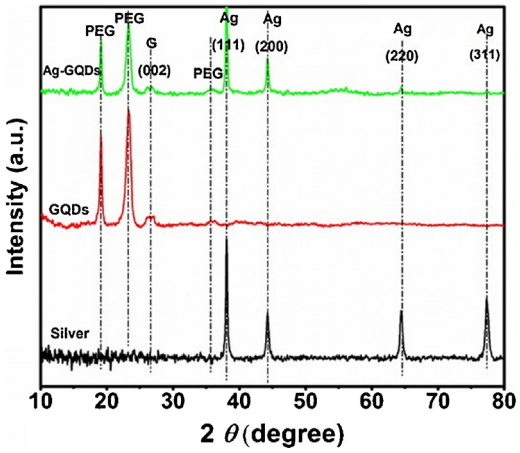

Fig. 2. XRD patterns of Ag-GQDs, GQDs and silver powder.

Ag-GQDs nanocomposites. The XRD results are consistent with the HR-TEM data described above.

The XPS technique was employed to quantify the approximate elemental composition attributed from silver and carbon in atomic percent (%). The XPS analyses indicate that the attribution of silver and carbon are approximately 33 and 66%, respectively. The deconvolution of the high resolution XPS spectrum at C1s (Fig. 3A) reveals the presence of amine, hydroxyl, ether and carboxyl groups at 285.9, 286.7, 287.7 and 289.4 eV, respectively. Fig. 3B shows the XPS signature of the Ag 3d doublet ($3d_{5/2}$ and $3d_{3/2}$) for the silver in the Ag-GQDs. The analyses of Ag 3d shows the presence of two Ag 3d doublets at 368.4 eV and 374.4 eV, and 369.8 eV and 375.8 eV, respectively. It is clear that both doublets are shifted to higher binding energy compared to metallic silver (368.2 eV) [35,36], which may be due to the electron transfer from metallic Ag to GQDs owing to the smaller work function of Ag than graphene. For the second resolved peak at 369.8 eV of the second doublet, the shift to higher binding energy compared to metallic silver could be assigned to a charge transfer between the silver and the polymer *i.e.*, PEG coating the nanocomposites [61].

The dispersion stability of Ag-GQDs was tested using the dynamic light scattering (DLS) technique. The DLS spectrum of the bare Ag-NPs (Fig. S1A) shows that they have a mean hydrodynamic diameter of 143.6 nm and the polydispersity index (PDI) is 0.327, which indicates that they are polydisperse and their large diameter is probably due to their tendency to agglomerate. On the other hand, the Ag-GQDs show a mean diameter of 33 nm and the PDI decreased *i.e.*, 0.095, as compared to the commercial Ag-NPs (Fig. S1B). The DLS data reveal that the PEGylation and the decoration of silver nanoparticles with GQDs increase the stability of silver and decrease their agglomeration.

3.2. Antibacterial activity tests

To evaluate the applicability of Ag-GQDs as an antibacterial agent, we tested them at different concentrations against *P. aeruginosa* and *S. aureus*. We employed the microdilution method to evaluate their antibacterial activity and to determine their minimum inhibitory concentration (MIC). The evaluation included also different concentrations of bare GQDs and Ag-NPs, in order to compare and analyze the antibacterial behavior contributed from each component of the nanocomposites. Table 1 summarizes the MIC values of bare Ag-NPs, bare GQDs and Ag-GQDs to inhibit both bacterial strains. The obtained data show that a MIC of 25 and 50 μg/mL of Ag-GQDs are required to inhibit the growth of *S. aureus* and *P. aeruginosa* bacteria, respectively. On the other hand, the MIC corresponding to bare Ag-NPs and GQDs were found to be above the tested concentrations of both nanoparticles (*i.e.*, >900 μg/mL for GQDs and >200 μg/mL for Ag-NPs). It is clear that there is a significant enhancement and a strong antibacterial activity associated with Ag-GQDs, as compared to bare Ag-NPs and GQDs.

Table 1
MIC values of Ag-GQDs, bare GQDs and bare Ag-NPs required for inhibition of *P. aeruginosa* and *S. aureus*.

Tested sample	MIC (μg/mL)	
	P. aeruginosa	*S. aureus*
GQDs	>900	>900
Ag-GQDs	50	25
Ag-NPs	>200	>200

We performed the fractional inhibitory concentration (FIC) test to evaluate the synergism between Ag and GQDs [46]. We took the MIC values of 200 and 900 μg/mL as the lower bounds for Ag-NPs and GQDs, respectively. The calculation gives an upper bound of the FIC index value of 0.31 and 0.15 for *P. aeruginosa* and *S. aureus*, respectively. According to Ruden et al. [59], a FIC index below 0.5 indicates synergy. Therefore, the results of the FIC test indicate that there is a synergistic effect between Ag-NPs and GQDs.

Moreover, to study the antimicrobial effectiveness of Ag-GQDs, dose-dependent growth kinetics curves of *P. aeruginosa* were used to assess the relative rate and extent of antibacterial activity of Ag-GQDs. Fig. S2A–C (see supplementary information) display the growth profiles of *P. aeruginosa* treated with various concentrations of bare Ag-NPs, GQDs, and Ag-GQDs. Fig. S2A shows a weak inhibition of *P. aeruginosa* when treated with bare Ag-NPs. The interaction between GQDs and *P. aeruginosa* was even weaker than bare Ag-NPs, and the inhibition was very low (see Fig. S2B). The highest concentration of 200 μg/mL induced a delay of 4 h in the growth rate of *P. aeruginosa*. On the other hand, Ag-GQDs nanocomposites displayed a considerably strong antibacterial behavior at lower concentrations. The treatment of *P. aeruginosa* with a concentration of 25 μg/mL induced a delay of 8 h in the bacterial population growth rate, and no growth was observed at higher concentrations for a period of 20 h.

We carried out similar bacterial population growth kinetics experiments for all tested nanoparticles with *S. aureus* (see Fig. S3A–C). High resistance was observed from *S. aureus* to bare Ag-NPs at all tested concentrations (see Fig. S3A). For bare GQDs, a low antibacterial activity against *S. aureus* was seen, where the bacterial growth rate becomes slower when increasing the GQDs concentrations. Nonetheless, an increase in the antibacterial effect of Ag-GQDs was observed, where the bacterial population growth was inhibited for at least 20 h at a concentration of 25 μg/mL.

Furthermore, we used the Kirby–Bauer method to evaluate the ability of Ag-GQDs nanocomposites to inhibit the formation of bacterial biofilms. Commonly commercial antibiotics (*i.e.*, ampicillin, streptomycin, and tetracycline) were used as positive inhibition control. Table 2 summarizes the diameter of the inhibition zones exhibited by the diffusion of Ag-GQDs, Ag-NPs, bare GQDs and

Table 2
Inhibition zones evaluated using the Kirby–Bauer method for: negative control, bare Ag-NPs, bare GQDs, Ag-GQDs and positive controls.

Tested sample	Inhibition zone (mm)	
	P. aeruginosa	*S. aureus*
Ag-GQDs (50 μg/disk)	10 ± 1	15 ± 1
Ag-GQDs (100 μg/disk)	24 ± 1	25 ± 0.5
GQDs (100 μg/disk)	–	–
Ag-NPs (50 μg/disk)	–	–
Ag-NPs (100 μg/disk)	–	–
Streptomycin	10 ± 0.1	15 ± 1
Tetracycline or ampicillin	20 ± 2	35 ± 1

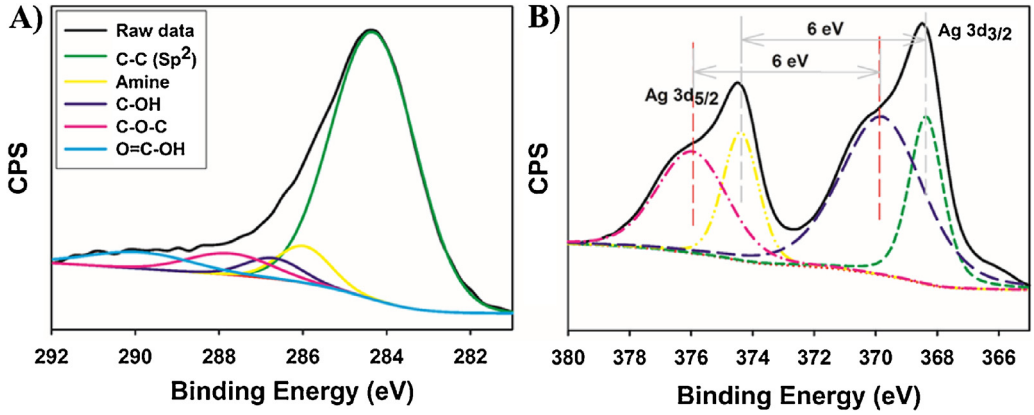

Fig. 3. High resolution XPS spectra of Ag-GQDs at (A) C1s. (B) Ag3d.

commercial antibiotics against *S. aureus* and *P. aeruginosa*. Ag-GQDs inhibited both bacterial strains at both concentrations, and the inhibition zones at the lowest concentration (50 μg/disk) are 10 and 15 mm for *P. aeruginosa* and *S. aureus*, respectively. In contrast, the bare GQDs and Ag-NPs did not exhibit any inhibition against both bacterial strains.

3.3. Proposed antibacterial mechanisms

Looking into the antibacterial activity of Ag-GQDs compared to bare GQDs and Ag-NPs, and the corresponding FIC test results described above, it is evident that the stronger antibacterial activity of Ag-GQDs arises from a synergistic effect between Ag-NPs and GQDs. To understand the origin of this synergistic effect, it is essential to analyze the possible interactions between bacteria and systems similar to Ag-GQDs (*i.e.*, Ag–CNTs, Ag–graphene, and Ag–graphene oxide).

There are several suggested mechanisms describing the bacterial inhibition by silver–carbon nanocomposites that have been proposed to explain the inhibition caused by Ag-GQDs. Kazmi et al. [30] suggest that the enhancement in the antibacterial properties of Ag-CNTs nanocomposites may result from silver ions (Ag^+) contributed by silver nanoparticles, which bind to thiol groups in enzymes and proteins on the cellular surface and cause destabilization of membranes and cellular walls. The size of the Ag-NPs is an essential factor in their ability to inhibit bacteria, since their MIC decreases when their size decreases [7,8]. This is due to the surface-to-volume ratio, which increases as the size decreases, and is consistent with the low antibacterial activity that we found for commercial bare Ag-NPs that aggregate into micron-scale clusters. Kazmi et al. [30] also suggested that the adhesion of Ag-NPs and CNTs composites to the bacterial cell wall can produce holes and allow the composite penetration inside the bacteria. The damage to the cell wall of bacteria by Ag-CNTs nanocomposites may also result from the interference in some physiological processes such as the downregulation of some genes associated with outer membrane integrity of the Gram-negative *Salmonella* bacteria [62]. Moreover, it was reported that nanostructures such as graphene, graphene oxide, CNTs and Ag-CNTs may induce considerable damage to the bacterial cell walls by oxidative stress induced by oxygen radicals and/or cell membrane disruption by sharp edges of graphene [15,17,33,53]. In fact, we observed physical damage to *P. aeruginosa* bacteria treated with Ag-GQDs in the SEM images (see Fig. S4). In Fig. S4A, the SEM image of untreated *P. aeruginosa* bacteria depicts their typical rod shape and 1–3 μm length. They underwent fragmentation and deformation after treatment with Ag-GQDs (see Fig. S4B). Akhavan et al. found that the cell membrane damage of the bacteria is induced by the direct contact of the bacteria with the extremely sharp edges of the nanowalls [15]. In this study, *Escherichia coli* bacteria with its outer membrane showed more resistance to the cell membrane damage caused by the nanowalls than *S. aureus*, which are lacking the outer membrane. This mechanism may explain the lower resistance of *S. aureus* to Ag-GQDs as compared to *P. aeruginosa*. Chook et al. reported that there is an enhancement in the antibacterial activity of reduced graphene oxide/silver nanocomposites due to an increase in the electron transfer rate from Ag-NPs to reduced graphene oxide, leading to the formation of partially positively charged Ag-NPs, which can enhance the inhibition effect [35]. This mechanism is supported by the XPS data obtained above that show a charge transfer between GQDs and Ag-NPs in Ag-GQDs nanocomposites. Marslin et al. reported that PEG facilitate the entry of nanoparticles carrying antibiotics, enhance the binding of the delivered drug to the bacterial DNA and block drug efflux pumps [55]. Since Ag-GQDs are PEGylated, it is possible that PEG enhance the entry of Ag-GQDs inside bacterial cells inhibition due to increasing of binding of DNA to silver. Another study suggested that the main advantage of silver–carbon nanostructures is to effectively stabilize Ag-NPs and prevent them from aggregation, which is a factor that greatly affects the effectiveness of Ag-NPs' antibacterial activities [63]. One or more of the above-described mechanisms may be simultaneously taking place to produce the synergistic antibacterial effect of Ag-GQDs.

3.4. Evaluation of cell viability in mammalian cells

We tested the cell viability of normal mammalian cells (*i.e.*, Vero cells) treated with Ag-GQDs, bare GQDs and bare Ag-NPs at the same concentrations used in the antibacterial activity tests after 24 h of incubation (Fig. 4A). The results show that cell viability was maintained at 100% for cells incubated with Ag-GQDs and bare GQDs for all the concentrations tested. Nevertheless, bare Ag-NPs have demonstrated a reduction in the cell viability for increasing concentrations. A 30% reduction in the cell viability was observed at a concentration of 150 μg/mL. Our results suggest that the decoration of Ag-NPs with GQDs may minimize the toxicity associated with silver nanoparticles.

Moreover, we have evaluated the cell viability of Ag-GQDs in two additional cells lines of human carcinoma (*i.e.*, HeLa and Jurkat cells). In HeLa cells, the cell viability remained at 100% for all the tested concentrations (see Fig. 4B). While testing the cell viability of Jurkat cells in the presence of Ag-GQDs we observed that cells maintained close to 100% for the bacterial MIC concentrations (25 and 50 μg/mL), however, a 50% reduction in the cell viability has been observed when a concentration of 150 μg/mL was used. It was reported by Eom et al. that Jurkat cells in particular are very

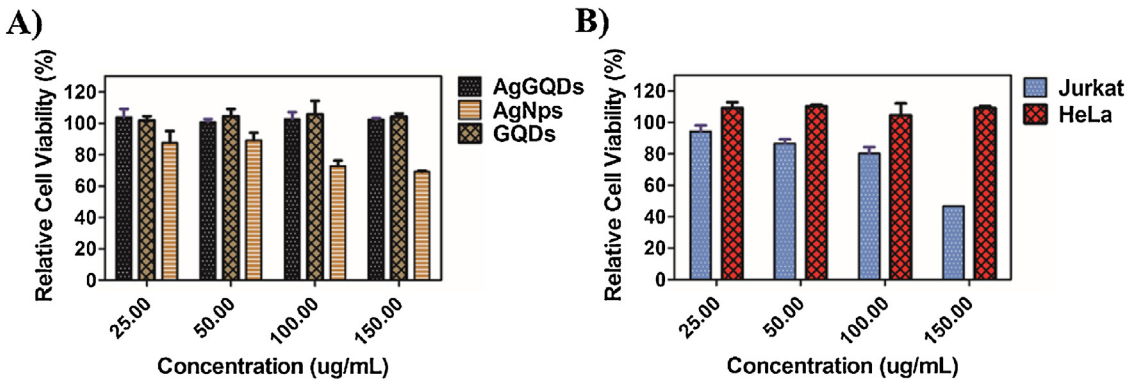

Fig. 4. MTS cell viability assay of: (A) Ag-GQDs, Ag-NPs and GQDs in Vero cells and (B) Ag-GQDs in Jurkat and HeLa cells. Data are presented as the mean ± SD from three independent experiments.

sensitive to Ag-NPs due to the activation of p38 MAPK, DNA damage, cell cycle arrest and apoptosis, and they report an almost 100% reduction in their viability when a concentration of 1 μg/mL was used [64]. This result indicates that coating the Ag-NPs with GQDs is an effective way to reduce their toxicity to mammalian cells.

4. Conclusions

We successfully synthesized biocompatible nanocomposites of Ag-GQDs consisting of Ag-NPs decorated with GQDs on their surface and functionalized with PEG. The Ag-GQDs showed enhanced antibacterial activity against *P. aeruginosa* and *S. aureus* bacteria, which are used as Gram-negative and Gram-positive model bacteria, respectively. The results showed that the decoration of Ag-NPs with GQDs fosters a synergistic effect and reduces dramatically the concentrations required to inhibit both bacterial strains, which are commonly isolated from microbial infections in wounds. The effective antibacterial concentrations of Ag-GQDs did not affect the viability of human and animal cells, which suggest that they are biocompatible and ecofriendly. These results also suggest that Ag-GQDs nanocomposites may be applied as antibacterial material, such as in: antibiotics, coating of surgical instrumentation, wound dressing textiles, disinfectants, antiseptic and detergents. Further studies are necessary in order to elucidate the exact mechanism(s) of Ag-GQDs that induce bacterial cytotoxicity.

Conflict of interest

The authors do not have any conflicts of interest to declare.

Acknowledgments

This research was carried out under the auspices of the Institute for Functional Nanomaterials (NSF Cooperative Agreement 1002410), PR NASA EPSCoR (NASA Cooperative Agreement NNX13AB22A), PR NASA Space Grant Consortium at University of Puerto Rico-Bayamon Campus (PRNSGC – UPRB), and UPR GK-12 Fellowship Program (NSF Grant No. 0841338). J.A. Gonzalez-Feliciano and D.P. Bracho-Rincon were supported by Molecular Sciences Research Center Fellowship. This work was also supported by PES funds from UPR to C.I. Gonzalez. We want to acknowledge Mr. Oscar Resto from the University of Puerto Rico – Rio Piedras Campus for taking HR-TEM images and Dr. Elizabeth Hunsperger from CDC for providing Vero cells.

Appendix A. Supplementary data

Supplementary data associated with this article can be found, in the online version, at doi:10.1016/j.apmt.2015.10.001.

References

[1] US Department of Health and Human Services, Centers for Disease Control and Prevention, Antibiotic Resistance Threats in the United States, 2013, US Centers for Disease Control and Prevention, 2013, http://www.cdc.gov/drugresistance/threat-report-2013/pdf/ar-threats-2013-508.pdf (accessed 24.01.15).
[2] P.G. Bowler, B.I. Duerden, D.G. Armstrong, Wound microbiology and associated approaches to wound management, Clin. Microbiol. Rev. 14 (2001) 244.
[3] T.J. Beveridge, Structures of Gram-negative cell walls and their derived membrane vesicles, J. Bacteriol. 181 (1999) 4725.
[4] M.A. Kohanski, D.J. Dwyer, J.J. Collins, How antibiotics kill bacteria: from targets to networks, Nat. Rev. Microbiol. 8 (2010) 423.
[5] J. Davies, D. Davies, Origins and evolution of antibiotic resistance, Microbiol. Mol. Biol. Rev. 74 (2010) 417.
[6] S. Agnihotri, S. Mukherji, S. Mukherji, Size-controlled silver nanoparticles synthesized over the range 5–100 nm using the same protocol and their antibacterial efficacy, RSC Adv. 4 (2014) 3974.
[7] N.V. Ayala-Núñez, H.H.L. Villegas, L.d.C.I. Turrent, C.R.g. Padilla, Silver nanoparticles toxicity and bactericidal effect against methicillin-resistant *Staphylococcus aureus*: nanoscale does matter, Nanobiotechnology 5 (2009) 2.
[8] M. Guzman, J. Dille, S.P. Godet, Synthesis and antibacterial activity of silver nanoparticles against Gram-positive and Gram-negative bacteria, Nanomed. Nanotechnol. 8 (2012) 37.
[9] C.N. Lok, C.M. Ho, R. Chen, Q.Y. He, W.Y. Yu, H. Sun, P.K.-H. Tam, J.F. Chiu, C.M. Che, Proteomic analysis of the mode of antibacterial action of silver nanoparticles, J. Proteome Res. 5 (2006) 916.
[10] S. Prabhu, E.K. Poulose, Silver nanoparticles: mechanism of antimicrobial action, synthesis, medical applications, and toxicity effects, Int. Nano Lett. 2 (2012) 1.
[11] M. Rai, A. Yadav, A. Gade, Silver nanoparticles as a new generation of antimicrobials, Biotechnol. Adv. 27 (2009) 76.
[12] M. Yamanaka, K. Hara, J. Kudo, Bactericidal actions of a silver ion solution on *Escherichia coli*, studied by energy-filtering transmission electron microscopy and proteomic analysis, Appl. Environ. Microbiol. 71 (2005) 7589.
[13] J.P. Ruparelia, A.K. Chatterjee, S.P. Duttagupta, S. Mukherji, Strain specificity in antimicrobial activity of silver and copper nanoparticles, Acta Biomater. 4 (2008) 707.
[14] A. Azam, A.S. Ahmed, M. Oves, M.S. Khan, A. Memic, Size-dependent antimicrobial properties of CuO nanoparticles against Gram-positive and -negative bacterial strains, Int. J. Nanomed. 7 (2012) 3527.
[15] O. Akhavan, E. Ghaderi, Toxicity of graphene and graphene oxide nanowalls against bacteria, ACS Nano 4 (2010) 5731.
[16] S. Kang, M. Herzberg, D.F. Rodrigues, M. Elimelech, Antibacterial effects of carbon nanotubes: size does matter!, Langmuir 24 (2008) 6409.
[17] S. Liu, T.H. Zeng, M. Hofmann, E. Burcombe, J. Wei, R. Jiang, J. Kong, Y. Chen, Antibacterial activity of graphite, graphite oxide, graphene oxide, and reduced graphene oxide: membrane and oxidative stress, ACS Nano 5 (2011) 6971.
[18] O. Medina, J. Nocua, F. Mendoza, R. Gomez-Moreno, J. Avalos, C. Rodriguez, G. Morell, Bactericide and bacterial anti-adhesive properties of the nanocrystalline diamond surface, Diam. Relat. Mater. 22 (2012) 77.
[19] B.Z. Ristic, M.M. Milenkovic, I.R. Dakic, B.M. Todorovic-Markovic, M.S. Milosavljevic, M.D. Budimir, V.G. Paunovic, M.D. Dramicanin, Z.M. Markovic, V.S. Trajkovic, Photodynamic antibacterial effect of graphene quantum dots, Biomaterials 35 (2014) 4428.
[20] H. Sun, N. Gao, K. Dong, J. Ren, X. Qu, Graphene quantum dots-band-aids used for wound disinfection, ACS Nano 8 (2014) 6202.
[21] A. Azam, A.S. Ahmed, M. Oves, M.S. Khan, S.S. Habib, A. Memic, Antimicrobial activity of metal oxide nanoparticles against Gram-positive and Gram-negative bacteria: a comparative study, Int. J. Nanomed. 7 (2012) 6003.

[22] D. Parsons, P.G. Bowler, V. Myles, S. Jones, Silver antimicrobial dressings in wound management: a comparison of antibacterial, physical, and chemical characteristics, Wounds 17 (2005) 222.
[23] S. Shahidi, J. Wiener, Antibacterial agents in textile industry, in: V. Bobbarala (Ed.), Antimicrobial Agents, INTECH, Rijeka, 2012, pp. 387–406, Available from: http://www.intechopen.com/books/antimicrobial-agents/antibacterial-agents-in-textile-industry.
[24] J. Zheng, J.D. Clogston, A.K. Patri, M.A. Dobrovolskaia, S.E. McNeil, Sterilization of silver nanoparticles using standard gamma irradiation procedure affects particle integrity and biocompatibility, J. Nanomed. Nanotechnol. (2011), 001.
[25] A. Abbaszadegan, Y. Ghahramani, A. Gholami, B. Hemmateenejad, S. Dorostkar, M. Nabavizadeh, H. Sharghi, The effect of charge at the surface of silver nanoparticles on antimicrobial activity against Gram-positive and Gram-negative bacteria: a preliminary study, J. Nanomater. 2015 (2015).
[26] Y. Matsumura, K. Yoshikata, S.i. Kunisaki, T. Tsuchido, Mode of bactericidal action of silver zeolite and its comparison with that of silver nitrate, Appl. Environ. Microbiol. 69 (2003) 4278.
[27] A. Burd, C.H. Kwok, S.C. Hung, H.S. Chan, H. Gu, W.K. Lam, L. Huang, A comparative study of the cytotoxicity of silver-based dressings in monolayer cell, tissue explant, and animal models, Wound Repair Regen. 15 (2007) 94.
[28] B.K. Kim, Y.L. Jo, J.J. Shim, Preparation and antibacterial activity of silver nanoparticles-decorated graphene composites, J. Supercrit. Fluids 72 (2012) 28.
[29] X. Dong, Y. Koo, Y. Tang, Y. Yun, L. Yang, Superior antibacterial activity of photochemical synthesized Ag–CNT composites and their synergistic effects in combination with other antimicrobial agents, J. Nanomed. Nanotechnol. 6 (2015) 2.
[30] S.J. Kazmi, M.A. Shehzad, S. Mehmood, M. Yasar, A. Naeem, A.S. Bhatti, Effect of varied Ag nanoparticles functionalized CNTs on its anti-bacterial activity against *E. coli*, Sens. Actuators A: Phys. 216 (2014) 287.
[31] Y. Seo, J. Hwang, J. Kim, Y. Jeong, M.P. Hwang, J. Choi, Antibacterial activity and cytotoxicity of multi-walled carbon nanotubes decorated with silver nanoparticles, Int. J. Nanomed. 9 (2014) 4621.
[32] W. Yuan, G. Jiang, J. Che, X. Qi, R. Xu, M.W. Chang, Y. Chen, S.Y. Lim, J. Dai, M.B. Chan-Park, Deposition of silver nanoparticles on multiwalled carbon nanotubes grafted with hyperbranched poly (amidoamine) and their antimicrobial effects, J. Phys. Chem. C 112 (2008) 18754.
[33] H. Yun, J.D. Kim, H.C. Choi, C.W. Lee, Antibacterial activity of CNT–Ag and GO–Ag nanocomposites against Gram-negative and Gram-positive bacteria, Bull. Korean Chem. Soc. 34 (2013) 3261.
[34] Q. Bao, D. Zhang, P. Qi, Synthesis and characterization of silver nanoparticle and graphene oxide nanosheet composites as a bactericidal agent for water disinfection, J. Colloid Interface Sci. 360 (2011) 463.
[35] S.W. Chook, C.H. Chia, S. Zakaria, M.K. Ayob, K.L. Chee, N.M. Huang, H.M. Neoh, H.N. Lim, R. Jamal, R.M.F.R.A. Rahman, Antibacterial performance of Ag nanoparticles and AgGO nanocomposites prepared via rapid microwave-assisted synthesis method, Nanoscale Res. Lett. 7 (2012) 1.
[36] K.C. Hsu, D.H. Chen, Microwave-assisted green synthesis of Ag/reduced graphene oxide nanocomposite as a surface-enhanced Raman scattering substrate with high uniformity, Nanoscale Res. Lett. 9 (2014) 1.
[37] W. Shao, X. Liu, H. Min, G. Dong, Q. Feng, S. Zuo, Preparation, characterization, and antibacterial activity of silver nanoparticle-decorated graphene oxide nanocomposite, ACS Appl. Mater. Interfaces 7 (2015) 6966.
[38] R. Foldbjerg, E.S. Irving, J. Wang, K. Thorsen, D.S. Sutherland, H. Autrup, C. Beer, The toxic effects of single-walled carbon nanotubes are linked to the phagocytic ability of cells, Toxicol. Res. 3 (2014) 228.
[39] C.w. Lam, J.T. James, R. McCluskey, S. Arepalli, R.L. Hunter, A review of carbon nanotube toxicity and assessment of potential occupational and environmental health risks, Crit. Rev. Toxicol. 36 (2006) 189.
[40] Y. Liu, Y. Zhao, B. Sun, C. Chen, Understanding the toxicity of carbon nanotubes, Acc. Chem. Res. 46 (2013) 702.
[41] C.A. Poland, R. Duffin, I. Kinloch, A. Maynard, W.A.H. Wallace, A. Seaton, V. Stone, S. Brown, W. MacNee, K. Donaldson, Carbon nanotubes introduced into the abdominal cavity of mice show asbestos-like pathogenicity in a pilot study, Nat. Nanotechnol. 3 (2008) 423.
[42] C.S. Sharma, S. Sarkar, A. Periyakaruppan, J. Barr, K. Wise, R. Thomas, B.L. Wilson, G.T. Ramesn, Single-walled carbon nanotubes induces oxidative stress in rat lung epithelial cells, J. Nanosci. Nanotechnol. 7 (2007) 2466.
[43] J. Tang, Q. Chen, L. Xu, S. Zhang, L. Feng, L. Cheng, H. Xu, Z. Liu, R. Peng, Graphene oxide–silver nanocomposite as a highly effective antibacterial agent with species-specific mechanisms, ACS Appl. Mater. Interfaces 5 (2013) 3867.
[44] Y. Chong, Y. Ma, H. Shen, X. Tu, X. Zhou, J. Xu, J. Dai, S. Fan, Z. Zhang, The in vitro and in vivo toxicity of graphene quantum dots, Biomaterials 35 (2014) 5041.
[45] J. Ge, M. Lan, B. Zhou, W. Liu, L. Guo, H. Wang, Q. Jia, G. Niu, X. Huang, H. Zhou, A graphene quantum dot photodynamic therapy agent with high singlet oxygen generation, Nat. Commun. 5 (2014) 4596.
[46] K. Habiba, V.I. Makarov, J. Avalos, M.J. Guinel, B.R. Weiner, G. Morell, Luminescent graphene quantum dots fabricated by pulsed laser synthesis, Carbon 64 (2013) 341.
[47] P. Li, F. Di Stasio, G. Eda, O. Fenwick, S.O. McDonnell, H.L. Anderson, M. Chhowalla, F. Cacialli, Luminescent properties of a water-soluble conjugated polymer incorporating graphene-oxide quantum dots, ChemPhysChem 16 (2015) 1258.
[48] M. Nurunnabi, Z. Khatun, K.M. Huh, S.Y. Park, D.Y. Lee, K.J. Cho, Y.k. Lee, In vivo biodistribution and toxicology of carboxylated graphene quantum dots, ACS Nano 7 (2013) 6858.
[49] P. Russo, A. Hu, G. Compagnini, W.W. Duley, N.Y. Zhou, Femtosecond laser ablation of highly oriented pyrolytic graphite: a green route for large-scale production of porous graphene and graphene quantum dots, Nanoscale 6 (2014) 2381.
[50] W. Shang, X. Zhang, M. Zhang, Z. Fan, Y. Sun, M. Han, L. Fan, The uptake mechanism and biocompatibility of graphene quantum dots with human neural stem cells, Nanoscale 6 (2014) 5799.
[51] L. Tang, R. Ji, X. Cao, J. Lin, H. Jiang, X. Li, K.S. Teng, C.M. Luk, S. Zeng, J. Hao, Deep ultraviolet photoluminescence of water-soluble self-passivated graphene quantum dots, ACS Nano 6 (2012) 5102.
[52] Z. Wang, H. Zeng, L. Sun, Graphene quantum dots: versatile photoluminescence for energy, biomedical, and environmental applications, J. Mater. Chem. C 3 (2014) 1157–1165.
[53] C. Wang, C. Wu, X. Zhou, T. Han, X. Xin, J. Wu, J. Zhang, S. Guo, Enhancing cell nucleus accumulation and DNA cleavage activity of anti-cancer drug via graphene quantum dots, Sci. Rep. 3 (2013).
[54] J.V. Jokerst, T. Lobovkina, R.N. Zare, S.S. Gambhir, Nanoparticle PEGylation for imaging and therapy, Nanomedicine 6 (2011) 715.
[55] G. Marslin, A.M. Revina, V.K.M. Khandelwal, K. Balakumar, C.J. Sheeba, G. Franklin, PEGylated ofloxacin nanoparticles render strong antibacterial activity against many clinically important human pathogens, Colloids Surf. B: Biointerface 132 (2015) 62–70.
[56] K. Habiba, V.I. Makarov, B.R. Weiner, G. Morell, Fabrication of nanomaterials by pulsed laser synthesis, in: W. Ahmed, N. Ali (Eds.), Manufacturing Nanostructures, One Central Press (OCN), Manchester, 2014, pp. 263–292.
[57] Clinical and Laboratory Standards Institute, M7-A7, Methods for Dilution Antimicrobial Susceptibility Tests for Bacteria That Grow Aerobically; Approved Standard, 7th ed., Wayne, PA, 2006.
[58] J.M. Andrews, Determination of minimum inhibitory concentrations, J. Antimicrob. Chemother. 48 (2001) 5.
[59] S. Ruden, K. Hilpert, M. Berditsch, P. Wadhwani, A.S. Ulrich, Synergistic interaction between silver nanoparticles and membrane-permeabilizing antimicrobial peptides, Antimicrob. Agents Chemother. 53 (2009) 3538.
[60] A. El Moussaoui, A. Chauvet, J. Masse, Etude des interactions a l'etat solide du nordazepam III-polyoxyethylene glycol 6000 et nordazepam III-acide succinique, J. Therm. Anal. Calorim. 39 (1993) 373.
[61] R. Zeng, M.Z. Rong, M.Q. Zhang, H.C. Liang, H.M. Zeng, Laser ablation of polymer-based silver nanocomposites, Appl. Surf. Sci. 187 (2002) 239.
[62] A.A. Chaudhari, S.L. Jasper, E. Dosunmu, M.E. Miller, R.D. Arnold, S.R. Singh, S. Pillai, Novel pegylated silver coated carbon nanotubes kill *Salmonella* but they are non-toxic to eukaryotic cells, J. Nanobiotechnol. 13 (2015) 23.
[63] S. Kumar-Krishnan, E. Prokhorov, M. Hernandez-Iturriaga, J.D. Mota-Morales, M. Vázquez-Lepe, Y. Kovalenko, I.C. Sanchez, G. Luna-Bárcenas, Chitosan/silver nanocomposites: synergistic antibacterial action of silver nanoparticles and silver ions, Eur. Polym. J. 67 (2015) 242.
[64] H.J. Eom, J. Choi, p38 MAPK activation, DNA damage, cell cycle arrest and apoptosis as mechanisms of toxicity of silver nanoparticles in Jurkat T cells, Environ. Sci. Technol. 44 (2010) 8337–8342.